



Article

Neonatal Extracellular Superoxide Dismutase Knockout Mice Increase Total Superoxide Dismutase Activity and VEGF Expression after Chronic Hyperoxia

Maxwell Mathias^{1,2,*} , Joann Taylor¹, Elizabeth Mendralla¹ and Marta Perez^{1,2}

¹ Division of Neonatology, Department of Pediatrics, Northwestern University Feinberg School of Medicine, Chicago, IL 60611, USA; j-hinz@northwestern.edu (J.T.); emendral@student.touro.edu (E.M.); mtperez@luriechildrens.org (M.P.)

² Ann & Robert H. Lurie Children's Hospital of Chicago, Chicago, IL 60611, USA

* Correspondence: maxwell-mathias@ouhsc.edu

Abstract: Bronchopulmonary dysplasia (BPD) is a common lung disease affecting premature infants that develops after exposure to supplemental oxygen and reactive oxygen intermediates. Extracellular superoxide dismutase (SOD3) is an enzyme that processes superoxide radicals and has been shown to facilitate vascular endothelial growth factor (VEGF) and nitric oxide (NO) signaling in vascular endothelium. We utilized a mouse model of neonatal hyperoxic lung injury and SOD3 knockout (KO) mice to evaluate its function during chronic hyperoxia exposure. Wild-type age-matched neonatal C57Bl/6 (WT) and SOD3^{-/-} (KO) mice were placed in normoxia (21% FiO₂, RA) or chronic hyperoxia (75% FiO₂, O₂) within 24 h of birth for 14 days continuously and then euthanized. Lungs were harvested for histologic evaluation, as well as comparison of antioxidant enzyme expression, SOD activity, VEGF expression, and portions of the NO signaling pathway. Surprisingly, KO-O₂ mice survived without additional alveolar simplification, microvascular remodeling, or nuclear oxidation when compared to WT-O₂ mice. KO-O₂ mice had increased total SOD activity and increased VEGF expression when compared to WT-O₂ mice. No genotype differences were noted in intracellular antioxidant enzyme expression or the NO signaling pathway. These results demonstrate that SOD3 KO mice can survive prolonged hyperoxia without exacerbation of alveolar or vascular phenotype.

Keywords: extracellular superoxide dismutase; bronchopulmonary dysplasia; vascular endothelial growth factor; nitric oxide signaling



Citation: Mathias, M.; Taylor, J.; Mendralla, E.; Perez, M. Neonatal Extracellular Superoxide Dismutase Knockout Mice Increase Total Superoxide Dismutase Activity and VEGF Expression after Chronic Hyperoxia. *Antioxidants* **2021**, *10*, 1236. <https://doi.org/10.3390/antiox10081236>

Academic Editor: Antonella Casola

Received: 2 July 2021

Accepted: 29 July 2021

Published: 1 August 2021

Publisher's Note: MDPI stays neutral with regard to jurisdictional claims in published maps and institutional affiliations.



Copyright: © 2021 by the authors. Licensee MDPI, Basel, Switzerland. This article is an open access article distributed under the terms and conditions of the Creative Commons Attribution (CC BY) license (<https://creativecommons.org/licenses/by/4.0/>).

1. Introduction

Bronchopulmonary dysplasia (BPD) is a common lung disease of prematurity, affecting more than 10,000 infants in the United States annually and up to 60% of infants born under 28 weeks [1,2]. BPD is a consequence of lung immaturity combined with the side-effects of life-sustaining therapeutic interventions, including supplemental oxygen (hyperoxia), which result in injury to the developing lung [3]. Hyperoxia is hypothesized to induce injury through the production of excess reactive oxygen intermediates (ROIs) [4]. Preterm infants are particularly susceptible to injury from ROI because of the immaturity of enzymatic antioxidant systems and relative deficiency of nonenzymatic antioxidants relative to term infants [5–9]. Because of the hypothesized causal pathway of hyperoxia–ROI–lung injury, there have been multiple clinical trials of administration of either antioxidant enzymes or nonenzymatic antioxidants; however, to date, none have demonstrated superiority over standard care or have received approval from the FDA [10–14]. Since these trials were conducted, our knowledge of cell-specific and compartment-specific redox signaling has vastly expanded, and it is clear that therapeutic intervention for neonatal hyperoxic lung injury (HLI) will require a more granular understanding of antioxidant system function during hyperoxia exposure [15].

Extracellular superoxide dismutase (SOD3) is an antioxidant enzyme found in high concentration in the lungs, and it is 95% tissue-bound at the interface between pulmonary vascular smooth muscle and pulmonary vascular endothelium [16,17]. SOD3 converts superoxide radical to hydrogen peroxide (H_2O_2), which can cross lipid bilayers and be converted to water by numerous intracellular antioxidant enzymes or can modify cysteine thiols on proteins for redox-dependent signaling [18]. SOD3 plays an important role in the development of the newborn lung. Its expression increases fivefold between weeks 1 and 3 of life and sevenfold between weeks 1 and 8 [5]. SOD3 knockout (KO) mice have simplified alveoli, pulmonary vascular remodeling, and increased susceptibility to bleomycin-induced lung injury at 3 and 4 weeks of life in comparison to controls [19–21]. In contrast, SOD3 overexpression protects against HLI in newborn animals, but does not appear to have any effect on alveolar or pulmonary vascular development during normoxia (21% FiO_2) [22–24]. The specific function of SOD3 in neonatal lung development and how this function is altered by hyperoxia exposure remains unknown.

One hypothesized function of SOD3 is that it protects nitric oxide (NO) signaling, whose function is critical to lung and pulmonary vascular development [24–28]. In the pulmonary vascular endothelium, NO is produced by the endothelial nitric oxide synthase (eNOS), diffuses into vascular smooth muscle, and binds soluble guanylate cyclase (sGC). Activated sGC catalyzes the conversion of GTP to cGMP, an important second messenger in vascular smooth muscle function and lung growth. Each step of this pathway has been shown to play an important role in early lung development, and sGC depletion has been shown to increase susceptibility to HLI [29–31]. SOD3 may protect NO bioavailability by reducing the extracellular concentration of superoxide, which can attack NO to form peroxynitrite ($ONOO^-$), itself a highly reactive and toxic intermediate [25,32,33]. In addition to direct effects on NO bioavailability, SOD3 can enhance NO signaling by increasing NO production in the vascular endothelium through its effect on vascular endothelial growth factor (VEGF) signaling. SOD3-derived H_2O_2 has been shown to potentiate the effect of VEGF on VEGF receptor 2 (VEGFR-2) phosphorylation [34]. VEGFR-2 phosphorylation induces the expression and activation of the endothelial nitric oxide synthase (eNOS), providing a link between the effects of SOD3 on VEGF and the NO signaling pathway [35,36].

In the present study, we evaluated the combined effects of SOD3 KO and chronic hyperoxia (O_2) on lung and pulmonary vascular development, and we tested the hypothesis that SOD3 protects lung development through VEGF-mediated effects on NO signaling. To our knowledge, this is the first study to investigate the effects of SOD3 KO on neonatal adaptations to chronic hyperoxia.

2. Materials and Methods

2.1. Animal Model

This study was approved by the Northwestern University Institutional Animal Care and Use Committee. SOD3^{-/-} mice (The Jackson Laboratory, Bar Harbor, ME, USA) were bred on a background of C57Bl/6N mice (Charles River, Wilmington, MA, USA) and back-crossed through multiple generations. Heterozygotes were then crossed to produce SOD3^{-/-} (KO) and SOD3^{+/+} (WT) offspring. Cages were checked daily for litters. New litters were placed in either room air (RA, 21% FiO_2) or a plexiglass chamber (Biospherix, Lacona, NY, USA) at 75% FiO_2 (Hyperoxia, or O_2) from birth to P14 continuously. Dams were rotated daily to prevent oxygen toxicity. Mice were euthanized at 14 days.

2.2. Tissue Collection and Processing

For histology, morphometry, and immunofluorescence, the chest was exposed, and lungs were removed en bloc and inflated to 25 cm H_2O with 10% formalin solution, fixed for 24 h, and paraffin-embedded. Blocks were cut into 5 μ m thick sections and stained with hematoxylin and eosin (H&E) for basic morphometry by the Northwestern University Mouse Histology and Phenotyping Laboratory and the Stanley Manne Children's Research

Institute Histology Laboratory. For Western blotting, enzyme activity assays, and immunoprecipitation, the RV was punctured, and the pulmonary artery was flushed with 3 mL of PBS to remove blood; then, the lung tissue was removed and snap-frozen in liquid nitrogen. Samples were stored at $-80\text{ }^{\circ}\text{C}$ until they were analyzed.

2.3. Lung Histology

H&E slides were blinded to the researcher. For alveolar area, 4–8 nonoverlapping images of the lungs were taken at $20\times$ magnification using an Olympus BX40 microscope (Olympus America, Melville, NY, USA) with a Moticam Pro 252A microscope camera (Motic, Kowloon, Hong Kong). Alveolar area was calculated using ImagePro 9.2 (Media Cybernetics, Rockland, MD, USA). Obvious airways and blood vessels were excluded, as were alveoli without complete borders. For pulmonary artery smooth muscle wall thickness index (MWT), 4–8 distinct resistance pulmonary arteries adjacent to airways measuring less than $100\text{ }\mu\text{m}$ diameter were photographed per slide at $40\times$ magnification. Inner and outer borders were traced in triplicate using ImageJ Software (ImageJ, NIH, Bethesda, MD, USA) to calculate circumference, and the ratio of smooth muscle to total area was compared between groups as described previously [37,38].

2.4. Immunofluorescence

Unstained $5\text{ }\mu\text{m}$ thick sections were obtained from paraffin-embedded lung samples. For von Willebrand Factor (vWF) immunofluorescence, slides were heated to $60\text{ }^{\circ}\text{C}$ for 10 min, and then cleaned and deparaffinized by serial dilutions of ethanol. Samples were then incubated in proteinase K solution (Sigma-Aldrich, St. Louis, MO, USA) for antigen retrieval at $37\text{ }^{\circ}\text{C}$ for 15 min. Samples were blocked with 5% bovine serum albumin (BSA; Sigma-Aldrich) in Tris-buffered saline containing 0.1% Tween-20 ($1\times$ TBST) at room temperature for 30 min, and then probed with von Willebrand Factor antibody (Agilent, Santa Clara, CA, USA; 1:50 in 5% BSA) overnight in a dark chamber. Slides were then washed in PBS twice and probed with Rhodamine Red conjugated goat anti-rabbit antibody (ThermoFisher, Waltham, MA, USA; 1:100 in 5% BSA) for 1 h in a dark chamber. Slides were again washed twice in PBS, blotted dry, and mounted prior to storage at $4\text{ }^{\circ}\text{C}$. Slides were imaged at $10\times$ magnification on a NIKON Eclipse TE300 fluorescent microscope and captured using a Photometrics SenSys KAF0400 G-2 camera. Eight nonoverlapping images per slide were obtained for vessel counts. Incompletely stained vessels or vessels with diameter $>100\text{ }\mu\text{m}$ were excluded.

8-Hydroxydeoxyguanosine (8-OHdG) is a product of DNA oxidation. To measure intracellular oxidative stress, 8-OHdG was quantified using immunofluorescence. Samples were deparaffinized on an automated platform (Leica Autostainer XL) and incubated in Sodium Citrate solution (pH 6) at $110\text{ }^{\circ}\text{C}$ for 10 min in a pressure cooker for antigen retrieval. Slides were then incubated in 8-OHdG antibody (Sigma-Aldrich, 1:100) overnight at $4\text{ }^{\circ}\text{C}$, washed, incubated in species-specific secondary antibody (Jackson ImmunoResearch, West Grove, PA, USA; 1:500), and counterstained with DAPI. Slides were imaged at $40\times$ magnification on a KEYENCE BZ-X fluorescent microscope (KEYENCE America, Itasca, IL, USA). A total of 4–8 nonoverlapping regions were selected, and duplicate images were obtained on blue (DAPI) and green (8-OHdG) channels. Images were converted to grayscale and analyzed using ImageJ. Nuclear borders were delineated by applying the same grayscale intensity threshold to all the DAPI images. These borders were overlaid on the 8-OHdG images, and the average 8-OHdG intensity of nuclear regions was calculated to filter out non-nuclear background fluorescence.

2.5. Western Blotting

Frozen lung tissue was crushed, suspended in protein lysis buffer (EMD Millipore Mg^{2+}) with phosphatase inhibitor and protease inhibitor (EMD Millipore and Sigma-Aldrich), and sonicated. Protein concentration was calculated using the Bradford method [39]. A total of 40 μg of protein lysate per sample was run on 4–20% gel (ThermoFischer) and transferred to

a nitrocellulose membrane (GE Life Sciences Amersham). Membranes were blocked with 5% BSA in TBST and incubated overnight with primary antibodies at 4 °C on a rocker. Membranes were washed and incubated with horseradish peroxidase (HRP)-conjugated, species-specific secondary antibodies, and again washed three times prior to imaging. SuperSignal West Femto Maximum Sensitivity Substrate (ThermoFischer Scientific, Rockford, IL, USA) was added, and chemiluminescence was detected using a molecular imager (BioRad, Hercules, CA, USA). Bands were analyzed using Image Lab (BioRad, Hercules, CA, USA), normalized to β -actin, and shown as fold difference relative to controls.

Primary antibodies were diluted in 5% BSA unless otherwise specified. Primary antibodies and concentrations used were as follows: SOD3 goat polyclonal antibody (pAb) at 1:1000 (R + D), cytosolic superoxide dismutase (SOD1) rabbit pAb at 1:1000 (Enzo P07632), mitochondrial superoxide dismutase (SOD2) rabbit pAb at 1:750 (Enzo P04179), glutathione peroxidase 1 (GPX-1) rabbit pAb at 1:1000 (Abnova 5038), catalase rabbit pAb at 1:2000 (Abcam ab52477), VEGF-A mouse monoclonal antibody (mAb) at 1:500 (Santa Cruz), sGC- α rabbit pAb at 1:2000 (Abcam), sGC- β rabbit pAb at 1:1000 (Cayman Chemical), endothelial nitric oxide synthase (eNOS) mouse mAb at 1:500 (Cayman Chemical), and β -actin rabbit mAb at 1:5000 (Cell Signaling). HRP-conjugated secondary antibodies and concentrations were as follows: goat anti-rabbit at 1:2000 (Cell Signaling), horse anti-mouse at 1:2000 (Cell Signaling), and donkey anti-goat at 1:2000 (Santa Cruz).

2.6. SOD Activity Assay

Protein lysates were obtained as described above. SOD enzyme activity was measured as described previously using a commercially available SOD Activity Kit (Enzo) [40]. Briefly, whole lung tissue lysates were passed through 0.45 μ m filter, and protein concentration was measured. A total of 150 μ g of lung protein was diluted to 75 μ L (2 μ g/ μ L) and incubated in SOD buffer, xanthine oxidase, and Water-Soluble Tetrazolium Salt 1 (WST-1) as per the manufacturer's instructions. Xanthine was added to initiate superoxide formation, which was measured as the rate of reduction of WST-1 to WST-1 formazan, which absorbs light at 450 nm. Absorbance readings were taken at 1 min intervals until WST-1 formazan formation ceased. SOD activity was calculated as rate of inhibition of WST-1 formazan formation. These were plotted against standard SOD enzyme concentrations (0.1 U/25 μ L to 10 U/25 μ L) on a logarithmic scale to estimate total SOD activity.

2.7. sGC Activity Assay

Protein lysates were obtained as described above. The cGMP ELISA kit was purchased from Cayman Chemical. A total of 30 μ g of protein was diluted to 100 μ L in incubation buffer consisting of 50 mM Tris-HCl (pH 7.5, Fisher Scientific), 4 mM MgCl₂ (Fisher Scientific), 0.5 mM 3-isobutyl-1-methylxanthine (Enzo), 7.5 mM creatine phosphate (Sigma-Aldrich), 0.2 mg/mL creatine phosphokinase (Sigma-Aldrich), 10 mM sodium nitroprusside (Sigma-Aldrich), and 1 mM GTP (Sigma-Aldrich) for 10 min at 37 °C. The reaction was terminated with 900 μ L of ice-cold 0.1 N HCl (Sigma-Aldrich) and then placed in a 90 °C water bath for 3 min to denature the protein. Samples were centrifuged for 15 min at 2000 \times g to precipitate protein. The supernatant was collected, dried in a speed vacuum, and resuspended in cGMP EIA buffer (Cayman Chemical, Ann Arbor, MI, USA). Samples were diluted 1:2 in EIA buffer for optimal calculation. Absorbance was detected at 405 nm using an iMark automated plate reader (BioRad, Hercules, CA, USA).

2.8. Statistics

Outliers were excluded using Grubb's test prior to analysis. Data are presented as means \pm SEM, and experimental groups were compared using Prism 8 software (GraphPad, San Diego, CA, USA) by two-way ANOVA with multiple comparisons, unless otherwise specified, to assess genotype and hyperoxia exposure effects and their interaction. Statistical significance was set at $p < 0.05$.

3. Results

3.1. Combined SOD3 KO and Hyperoxia Exposure Does Not Cause More Alveolar Simplification Than SOD3 KO or Hyperoxia Alone

Mean alveolar area for the control group (WT-RA) was $1055 \pm 41 \mu\text{m}^2$. SOD3 KO and hyperoxia exposure independently induced a significant increase in alveolar area, which was $1863 \pm 242 \mu\text{m}^2$ for the KO-RA group and $2932 \pm 270 \mu\text{m}^2$ for the WT-O₂ group (Figure 1A). The combination of SOD3 KO and hyperoxia exposure (KO-O₂ group) did not induce further alveolar simplification ($2364 \pm 134 \mu\text{m}^2$). Representative images are shown in Figure 1B.

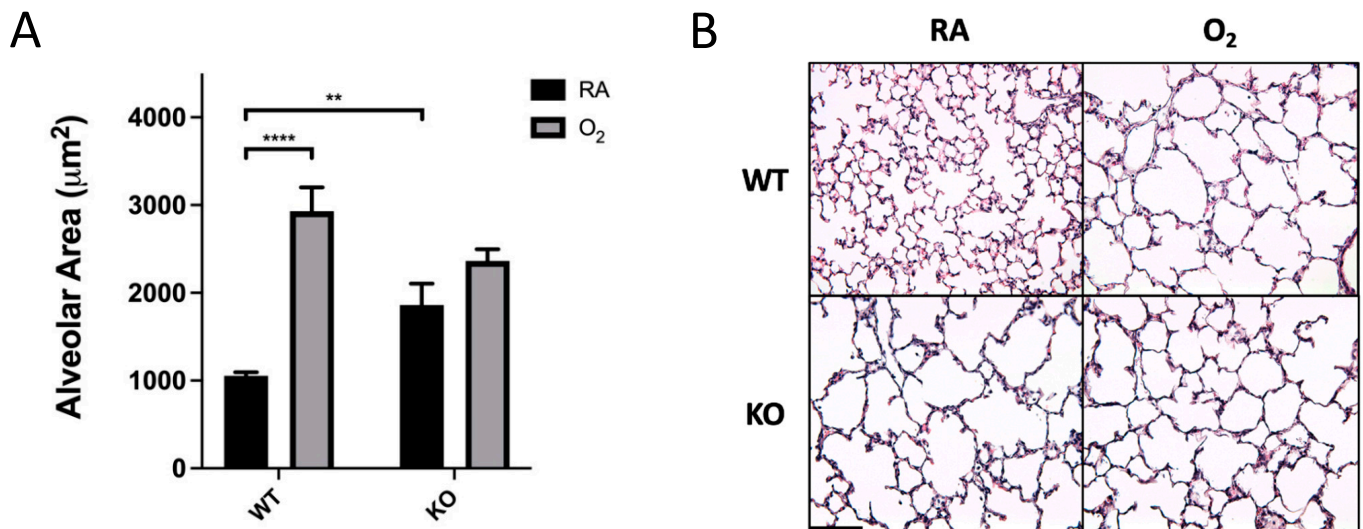


Figure 1. Hyperoxia exposure and SOD3 KO alone induced alveolar simplification, but there was no additive effect of genotype and exposure. (A) WT and KO mice were exposed to 14 days of either 75% O₂ or RA prior to analysis. Lungs were sectioned, H&E-stained, and analyzed at 20 \times magnification. Alveolar area was significantly higher in O₂-exposed mice in the WT genotype but not the KO genotype. Data are presented as \pm means SEM; ** $p < 0.01$, **** $p < 0.0001$; $n = 8$ –15 per group. (B) Representative (20 \times) images of H&E-stained P14 mouse lung. Scale bar is 100 μm .

3.2. Combined SOD3 KO and Hyperoxia Exposure Does Not Cause More Microvascular Remodeling Than SOD3 KO or Hyperoxia Alone

Pulmonary vascular MWT for WT-RA was 0.31 ± 0.006 . SOD3 KO and hyperoxia exposure independently induced a significant increase in MWT, which was 0.43 ± 0.03 for the KO-RA group and 0.42 ± 0.03 for the WT-O₂ group (Figure 2A). The combination of genotype and hyperoxia exposure did not induce a further increase in MWT (0.39 ± 0.03). Representative images are shown in Figure 2B. Mean vessel density as quantified by vWF-stained vessels per 10 \times field was 6.5 ± 0.6 in WT-RA. KO-RA and WT-O₂ both had decreased vessel density (4.1 ± 0.6 and 3.5 ± 0.4 , respectively; Figure 2C) compared to WT-RA. KO-O₂ mice showed no additional reduction in vascular density (Figure 2C). Representative phase-contrast and fluorescent images are shown in Figure 2D.

3.3. DNA Oxidation Was Not Affected by Genotype

There was an overall increase in 8-OHdG immunofluorescent intensity in hyperoxia-exposed mice; however, post hoc Tukey's test for multiple comparisons did not reach statistical significance (Figure 3A). There was no effect of genotype on DNA oxidation. Representative phase-contrast, fluorescent, and overlaid images are shown in Figure 3B.

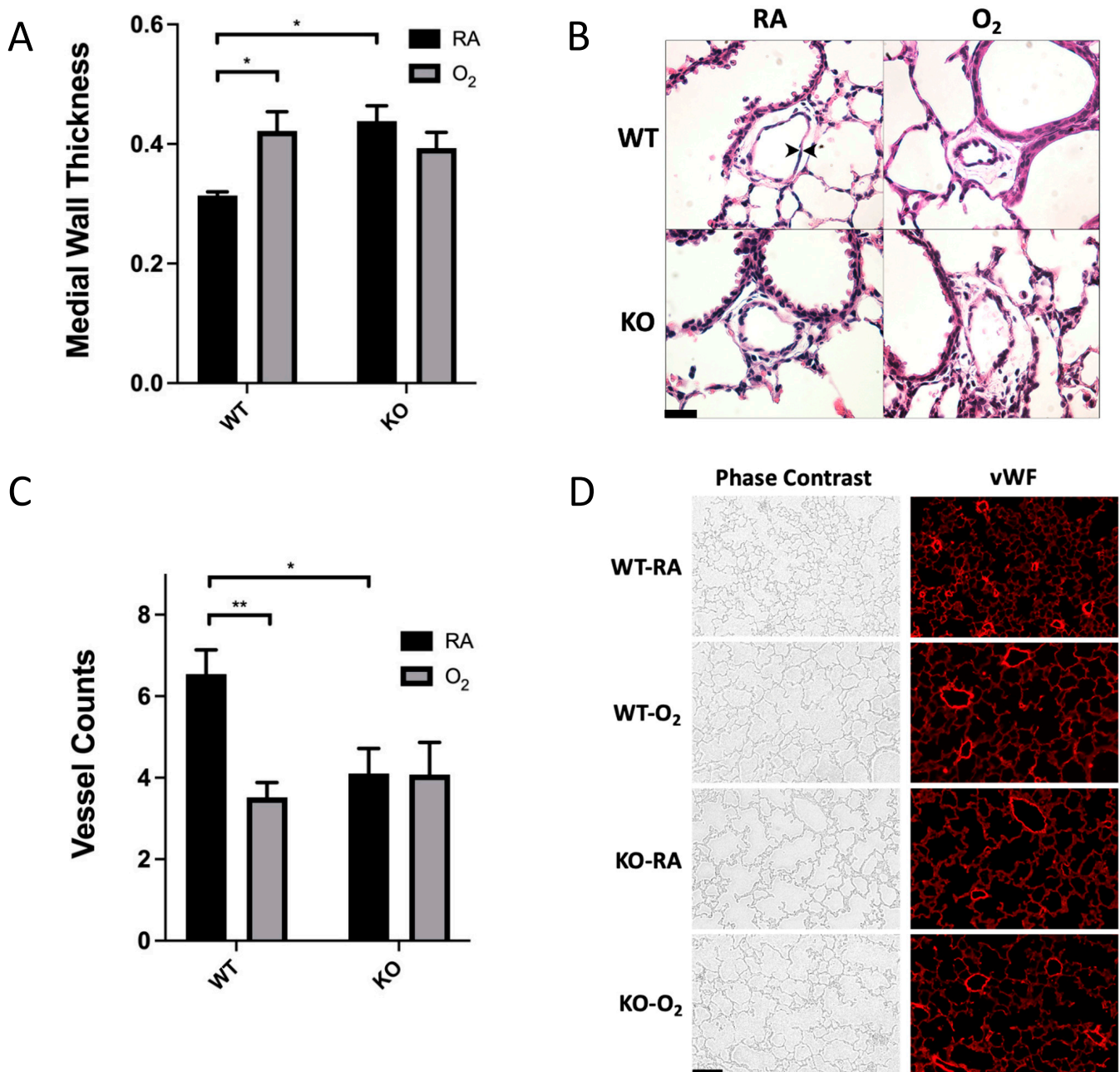


Figure 2. Hyperoxia exposure and SOD3 KO alone induced microvascular remodeling, but there was no additive effect of genotype and exposure. **(A)** Lung sections were analyzed at 40 \times magnification. Cross-sections of peri-bronchiolar arterioles were identified for analysis. Medial wall thickness was significantly higher in O₂-exposed mice in the WT genotype but not the KO genotype; $n = 5\text{--}7$. **(B)** Representative high-power (40 \times) images of H&E-stained cross-sections of peribronchiolar pulmonary arterioles. Arrowheads indicate the medial layer. Scale bar is 20 μm . **(C)** Lung sections were stained with vWF antibody to highlight the vascular endothelium. Vascular density was analyzed by counting resistance pulmonary blood vessels (<100 μm diameter) per low-power (10 \times) field. Vessel counts were significantly lower in O₂-exposed mice compared to RA in the WT genotype but not the KO genotype. **(D)** Representative low-power (10 \times) images of phase-contrast and immunofluorescent lung are presented. Scale bar is 100 μm . Data are presented as means \pm SEM; * $p < 0.05$, ** $p < 0.01$.

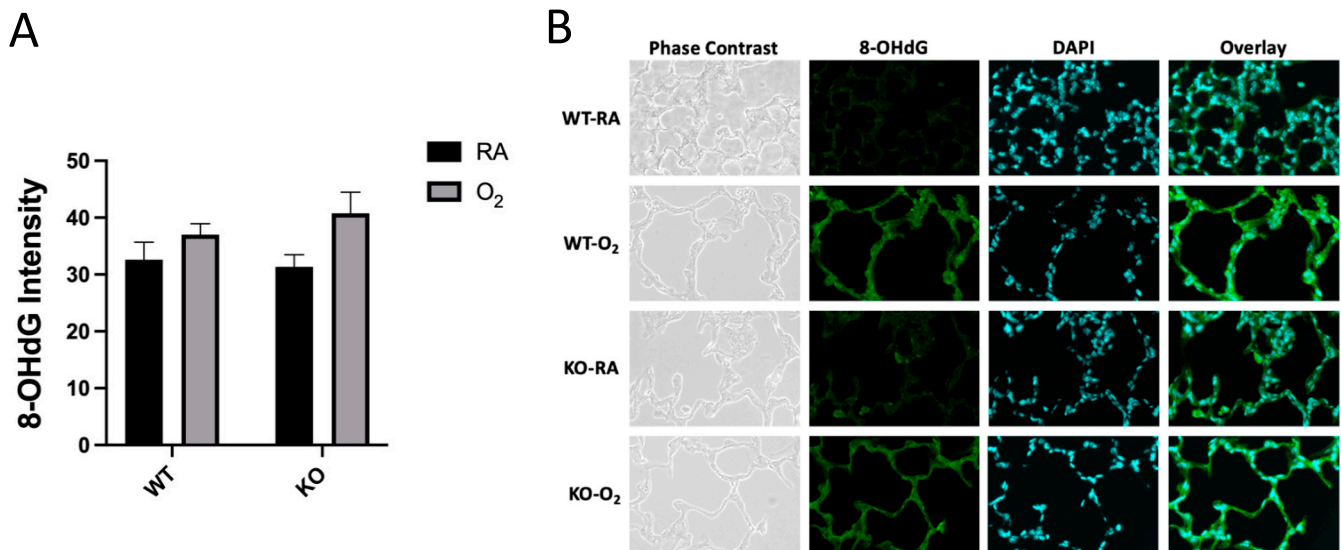


Figure 3. SOD3 KO did not affect DNA oxidation. (A) Lung sections were stained for 8-OHdG and counterstained with DAPI. Nuclei were identified on the basis of DAPI fluorescent intensity, and these regions were analyzed for 8-OHdG fluorescent intensity to avoid analyzing background autofluorescence. There was an overall increase in 8-OHdG fluorescent intensity in hyperoxia-exposed mice by two-way ANOVA ($p < 0.05$); however, post hoc individual group comparisons did not reach statistical significance. (B) Representative images of phase-contrast, 8-OHdG immunofluorescent (green), and DAPI-stained (blue) lungs are presented. An overlay of the 8-OHdG and DAPI images is shown in the far-right column.

3.4. SOD3 Protein Was Absent in KO Mice, but Genotype Did Not Affect Other Antioxidant Protein Expression

There was no SOD3 protein detected in the KO mice, along with no effect of O₂ exposure on SOD3 expression. In addition to SOD3, SOD1, SOD2, GPX-1, and catalase expression was assayed by Western blot (Figure 4A). Hyperoxia exposure increased SOD2 expression in both WT and KO mice (1.0 ± 0.1-fold vs. 2.6 ± 0.2-fold in WT; 0.9 ± 0.1-fold vs. 1.9 ± 0.3-fold in KO), as described previously [40]. Hyperoxia exposure also decreased catalase expression in WT mice (1.0 ± 0.03-fold vs. 0.72 ± 0.06-fold). However, there was no effect of genotype on measured antioxidant enzyme expression between groups. Representative blots are shown in Figure 4B.

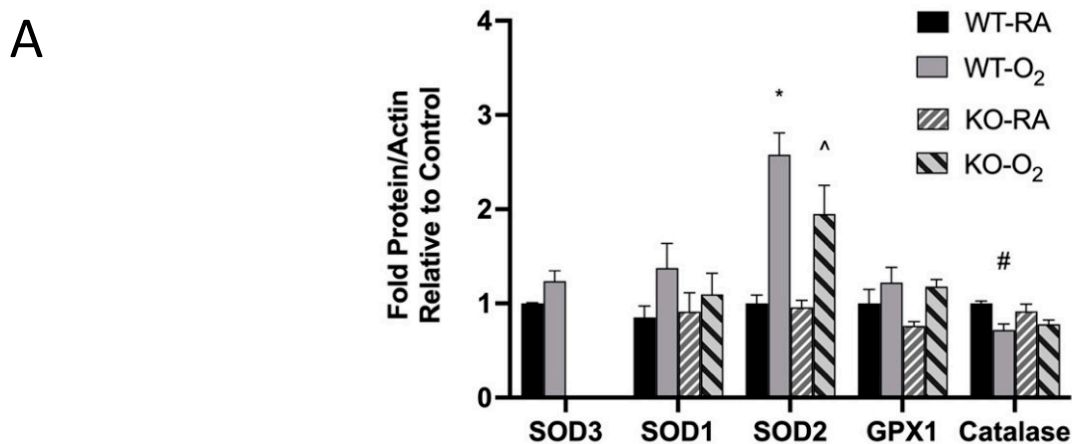


Figure 4. Cont.

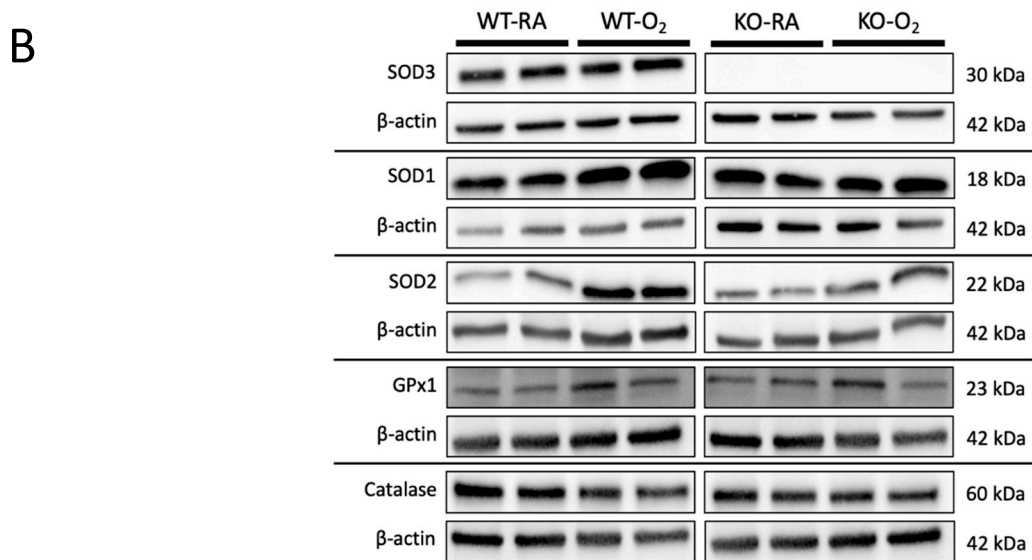


Figure 4. SOD3 protein was absent in KO mice, but other antioxidant enzyme expression was not affected by genotype. (A) Western blot analysis was used to evaluate lung protein expression of SOD3, SOD1, SOD2, GPX-1, and catalase in WT and KO mice exposed to either RA or O₂ for 14 days. Protein expression was normalized to β-actin. No SOD3 protein was detected in KO mice, and O₂ exposure did not affect SOD3 expression in WT mice. O₂ exposure was associated with increased SOD2 expression in both genotypes (as previously described [1]) and decreased catalase expression in WT mice. Data are presented as means ± SEM; * $p < 0.0001$ vs. WT RA, ^ $p < 0.05$ vs. WT RA, # $p < 0.01$ vs. KO RA, by two-way ANOVA with multiple comparisons; $n = 4-6$ per group. (B) Representative blot images are presented.

3.5. Combined SOD3 KO and Hyperoxia Increased Total SOD Activity

KO-O₂ mice had increased total SOD activity when compared to WT-O₂ mice (77.1 ± 4.2 vs. 60.0 ± 4.5 mU SOD activity/μg protein; Figure 5). Comparison of KO-RA and KO-O₂ mice did not reach statistical significance (63.5 ± 3.8 vs. 77.1 ± 4.2 mU SOD activity/μg protein, $p = 0.06$).

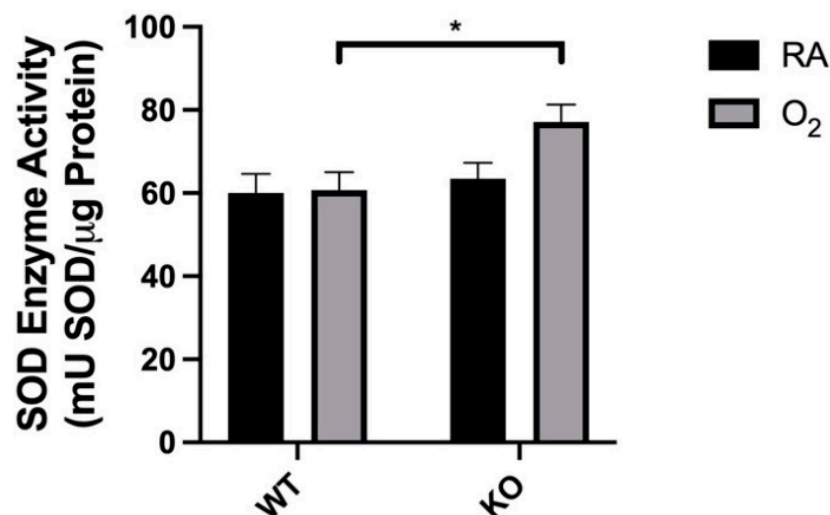


Figure 5. Total SOD activity was increased in KO-O₂ mice. SOD activity was measured as the rate of elimination of superoxide compared to standard concentrations of SOD enzyme. Whole-lung SOD enzyme activity was increased only in KO-O₂ mice. Data are presented as means ± SEM; * $p < 0.05$ vs. WT O₂; $n = 6-9$ per group.

3.6. KO-O₂ Mice Increased VEGF and Decreased eNOS in Response to Hyperoxia

KO-O₂ mice had increased VEGF expression when compared to WT-O₂ mice (2.7 ± 0.4 -fold vs. 1.5 ± 0.1 -fold; Figure 6A). In order to evaluate downstream effects on the NO-signaling pathway, we assessed eNOS and sGC protein subunit expression and sGC function (Figure 6B–D). eNOS expression was decreased in O₂-exposed KO mice but not WT mice. sGC- α and - β expression were both significantly reduced in the O₂ groups (sGC- α not shown), but there was no genotype effect. Representative blots for VEGF, eNOS, and sGC- β are shown. Despite protein expression differences, there were no significant group differences in measured sGC activity (Figure 6D).

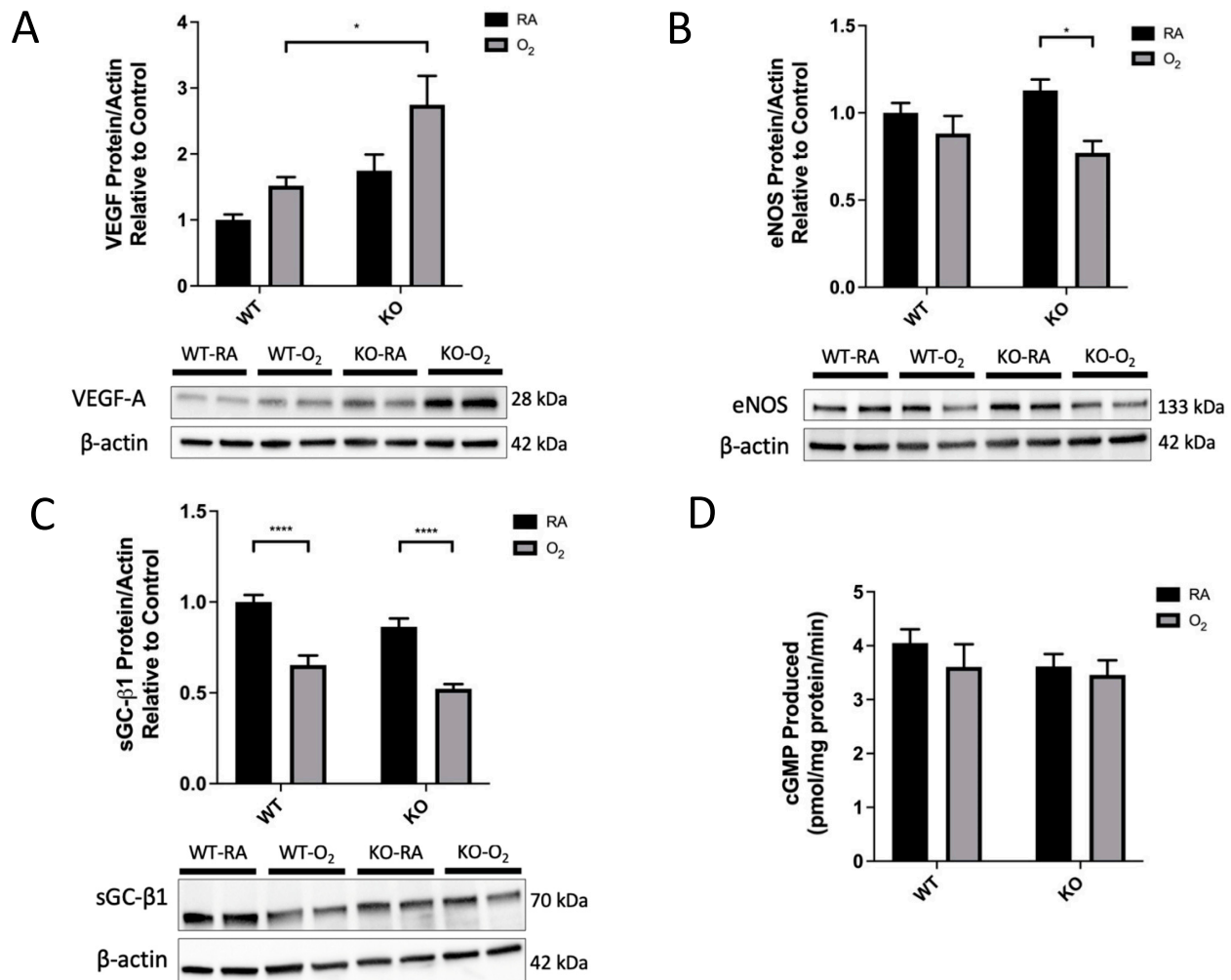


Figure 6. VEGF was increased and eNOS was decreased in combined SOD3 KO and hyperoxia. Western blot analysis was used to evaluate lung protein expression of VEGF-A, eNOS, and sGC- β 1 in WT and KO mice exposed to either RA or O₂ for 14 days. Protein expression was normalized to β -actin. Representative blots are presented. (A) VEGF-A expression was significantly increased by the combination of O₂ and SOD3 KO. (B) eNOS expression was significantly decreased by the combination of O₂ and SOD3 KO. (C) sGC- β 1 expression was decreased in both genotypes following O₂ exposure, but there was no genotype effect. sGC- α protein was also measured and had an identical expression pattern (data not shown). (D) sGC activity was measured in whole-lung lysates and was not affected by O₂ exposure or genotype. Data are presented as means \pm SEM; * $p < 0.05$, **** $p < 0.0001$ vs. WT RA; $n = 4$ –8 per group.

4. Discussion

SOD3 has been identified as an antioxidant enzyme whose excess is protective of hyperoxic lung injury and whose absence induces histologic changes similar to those seen in hyperoxic lung injury [19,20,23]. However, the precise function of SOD3 and how this

function is affected by hyperoxia remains understudied in the neonatal lung. In the present study, neonatal SOD3 KO mice survive prolonged hyperoxia without exacerbation of alveolar simplification or vascular remodeling that occurs in hyperoxia-exposed WT mice or KO mice in RA (Figure 1; Figure 2). These results are surprising, as both hyperoxia exposure and SOD3 KO alone induce significant damage to alveoli and pulmonary vasculature.

One possibility for these findings is that SOD3 KO induces changes to alveoli and pulmonary vasculature through local effects on redox state in the extracellular space, while hyperoxia exposure induces changes through mitochondrial reactive oxygen species production [41]. We found overall increased nuclear DNA oxidation in hyperoxia-exposed mice but did not find any genotype differences (Figure 3). The lack of increased DNA oxidation in KO mice could mean that local changes in redox state in SOD3 KO are alone sufficient for the phenotypic changes seen in more global “oxidative stress”. This hypothesis is supported by the fact that a delocalizing mutation that converts arginine to glycine (R213G) allows SOD3 to retain enzymatic function, but induces similar morphologic changes in the pulmonary vasculature [42].

If global hyperoxia exposure and SOD3 KO induce similar phenotypic changes through different mechanisms (local extracellular redox state vs. mitochondrial ROI), then why did the dual hit KO-O₂ mice not exhibit a worse phenotype? We hypothesized that these mice adapt through upregulation of alternative antioxidants. While we found no differences in measured SOD protein expression (Figure 4), our results demonstrate increased total SOD activity in KO-O₂ mice when compared to WT-O₂ mice (Figure 5). One possibility for this discrepancy between protein expression and activity is post-translational modification. Numerous post-translational modifications to SODs, including by reactive oxygen and nitrogen species (such as ONOO⁻), have been shown to inhibit SOD1 and SOD2, although limited study has been done on SOD3 [43]. Another hypothesis for the observed lack of phenotypic differences between WT and SOD3 KO mice exposed to hyperoxia is that SOD3 KO and oxygen exposure cause phenotypic changes through a common pathway that is maximally affected by SOD3 KO or O₂ exposure. The phenotype of KO-RA mice suggests some degree of baseline injury that may activate the transcription factor nuclear factor erythroid 2-related factor 2 (NRF2). NRF2 is a redox-sensitive regulator of myriad antioxidant genes, including SOD3 [44,45]. It is not known, however, whether SOD3 KO activates NRF2, which would confer resistance to further oxidative stress in the SOD3 KO mice. Further study is needed to investigate these possibilities, as well as the importance of post-translational modifications of SOD enzymes on hyperoxic responses in neonatal lungs.

We initially hypothesized that SOD3 protects lung development through VEGF-mediated effects on NO signaling. In a study using 7 days of postnatal exposure at 95% FiO₂, Perveen et al. found decreased pulmonary VEGF-A protein and vascular endothelial progenitor cell population density in neonatal O₂-exposed mice [24]. In the same model, SOD3 overexpression protected against these hyperoxic changes. Interestingly, we did not find decreased VEGF-A protein expression in WT mice after O₂ exposure in our model but did see significantly increased VEGF-A protein in KO mice after O₂ exposure (Figure 6A). In addition, our KO mice demonstrated decreased eNOS expression after O₂ exposure that was not seen in WT mice (Figure 6B).

Indeed, eNOS expression has been shown to be decreased in a lamb model of persistent pulmonary hypertension of the newborn (PPHN) only after O₂-exposure but not in RA, and eNOS expression was restored in these PPHN-O₂ lambs with exogenous SOD administration [28]. Lastly, decreased eNOS expression in the KO-O₂ mice compared to KO-RA animals was not associated with altered sGC activity despite reduced sGC expression (Figure 6B–D). Contrary to our initial hypothesis, this would suggest that NO-independent pathways are responsible for the phenotypic differences between WT and KO mice and for the adaptation of the KO-O₂ mice to the dual hit. NO-independent pathways stimulated by VEGF might contribute to relative attenuation of hyperoxic lung injury in our KO mice, and this deserves further study [46,47].

There are several limitations to the present study. Firstly, as it relates to animal models of bronchopulmonary dysplasia, the study was designed to be narrow in scope and assess only the effect of hyperoxia exposure and a single antioxidant enzyme, SOD3. BPD is a chronic illness that results from prematurity combined with prenatal exposures, inflammation, oxygen exposure, mechanical lung injury, genetic predisposition, and nutritional status, among other factors. In addition, neonatal hyperoxic lung injury involves far broader and more complex mechanisms than can be elucidated in a single gene knockout.

Secondly, we used a global SOD3 knockout rather than a tissue- or cell-specific knockout. SOD3 is expressed in vascular smooth muscle throughout the body and has been used to model disease processes in other organ systems, including the kidneys [48], eyes [49], and ischemia/reperfusion [50]. However, SOD3 is found in highest content per gram tissue in the vasculature of the lungs, and, despite global knockout, these mice otherwise have a normal lifespan [20]. In addition, we demonstrated decreased eNOS expression in KO-O₂ mice, but did not assess eNOS activity, which might be affected by factors unrelated to protein expression [51]. Lastly, enzyme activity assays can be limited in their generalizability to in vivo function. Features such as substrate and cofactor concentrations, post-translational modifications, and compartmentalization can all affect enzymatic function in ways that we did not assess.

5. Conclusions

We demonstrated that SOD3 KO mice survive prolonged hyperoxia without exacerbation of HLI phenotype. This survival is associated with increased overall SOD activity and increased VEGF expression. Further study is needed to assess whether these mice survive the dual hit due to a common pathway affected by SOD3 KO and hyperoxia exposure or by adaptation through upregulation of SOD activity and/or NO-independent VEGF signaling.

Author Contributions: Conceptualization, M.M. and M.P.; methodology, M.M., J.T., E.M., and M.P.; formal analysis, M.M., J.T., and M.P.; investigation, M.M., E.M., J.T., and M.P.; resources, M.P.; writing—original draft preparation, M.M.; writing—review and editing, M.M., J.T., E.M., and M.P.; visualization, M.M.; supervision, M.P.; funding acquisition, M.M. and M.P. All authors read and agreed to the published version of the manuscript.

Funding: This research was funded by the National Heart, Lung, and Blood Institute (grant K08HL124295 to M.P.) and the Little Giraffe Foundation Neonatal Research Grant (to M.M.).

Institutional Review Board Statement: This study was approved by the Northwestern University Animal Care and Use Committee (Protocol IS4076).

Informed Consent Statement: Not applicable.

Data Availability Statement: A supplemental figure is available on FigShare at <http://doi.org/10.6084/m9.figshare.15109872>. All other data are contained within the article.

Acknowledgments: Histology services were provided by the Northwestern University Mouse Histology and Phenotyping Laboratory, which is supported by NCI CCSG P30 CA060553, awarded to the Robert H. Lurie Comprehensive Cancer Center. Gregory Waypa provided guidance on 8-OHdG immunofluorescence analysis.

Conflicts of Interest: The authors declare no conflict of interest.

References

1. Stroustrup, A.; Trasande, L. Epidemiological Characteristics and Resource Use in Neonates With Bronchopulmonary Dysplasia: 1993–2006. *Pediatrics* **2010**, *126*, 291–297. [CrossRef]
2. Poindexter, B.B.; Feng, R.; Schmidt, B.; Aschner, J.L.; Ballard, R.A.; Hamvas, A.; Reynolds, A.M.; Shaw, P.A.; Jobe, A.H. Prematurity and Respiratory Outcomes Program Comparisons and Limitations of Current Definitions of Bronchopulmonary Dysplasia for the Prematurity and Respiratory Outcomes Program. *Ann. Am. Thorac. Soc.* **2015**, *12*, 1822–1830. [CrossRef]
3. Baraldi, E.; Filippone, M. Chronic Lung Disease after Premature Birth. *N. Engl. J. Med.* **2007**, *357*, 1946–1955. [CrossRef]
4. Saugstad, O.D. Bronchopulmonary Dysplasia-Oxidative Stress and Antioxidants. *Semin. Neonatol.* **2003**, *8*, 39–49. [CrossRef]

5. Berkelhamer, S.K.; Kim, G.A.; Radder, J.E.; Wedgwood, S.; Czech, L.; Steinhorn, R.H.; Schumacker, P.T. Developmental Differences in Hyperoxia-Induced Oxidative Stress and Cellular Responses in the Murine Lung. *Free Radic. Biol. Med.* **2013**, *61*, 51–60. [[CrossRef](#)]
6. Heinonen, K.; Mononen, I.; Mononen, T.; Parviainen, M.; Penttilä, I.; Launiala, K. Plasma Vitamin C Levels Are Low in Premature Infants Fed Human Milk. *Am. J. Clin. Nutr.* **1986**, *43*, 923–924. [[CrossRef](#)]
7. Ochoa, J.J.; Ramirez-Tortosa, M.C.; Palomino, N.; Robles, R.; Mataix, J.; Huertas, J.R.; Quiles, J.L. Oxidative Stress in Erythrocytes from Premature and Full-Term Infants During Their First 72 h of Life. *Free Radic. Res.* **2003**, *37*, 317–322. [[CrossRef](#)]
8. Autor, A.P.; Frank, L.; Roberts, R.J. Developmental Characteristics of Pulmonary Superoxide Dismutase: Relationship to Idiopathic Respiratory Distress Syndrome. *Pediatric Res.* **1976**, *10*, 154–158. [[CrossRef](#)] [[PubMed](#)]
9. Ofman, G.; Tipple, T.E. Antioxidants & Bronchopulmonary Dysplasia: Beating the System or Beating a Dead Horse? *Free Radic. Biol. Med.* **2019**, *142*, 138–145. [[CrossRef](#)]
10. Rosenfeld, W.; Evans, H.; Concepcion, L.; Jhaveri, R.; Schaeffer, H.; Friedman, A. Prevention of Bronchopulmonary Dysplasia by Administration of Bovine Superoxide Dismutase in Preterm Infants with Respiratory Distress Syndrome. *J. Pediatrics* **1984**, *105*, 781–785. [[CrossRef](#)]
11. Davis, J.M.; Parad, R.B.; Michele, T.; Allred, E.; Price, A.; Rosenfeld, W. Pulmonary Outcome at 1 Year Corrected Age in Premature Infants Treated at Birth With Recombinant Human CuZn Superoxide Dismutase. *Pediatrics* **2003**, *111*, 469–476. [[CrossRef](#)]
12. Suresh, G.; Davis, J.M.; Soll, R. Superoxide Dismutase for Preventing Chronic Lung Disease in Mechanically Ventilated Preterm Infants. *Cochrane Database Syst. Rev.* **2001**. [[CrossRef](#)]
13. Buonocore, G.; Groenendaal, F. Anti-Oxidant Strategies. *Semin. Fetal Neonatal Med.* **2007**, *12*, 287–295. [[CrossRef](#)]
14. Jr, C.A.S.; McEvoy, C.T.; Aschner, J.L.; Kirk, A.; Rosas-Salazar, C.; Cook-Mills, J.M.; Moore, P.E.; Walsh, W.F.; Hartert, T.V. Update on Vitamin E and Its Potential Role in Preventing or Treating Bronchopulmonary Dysplasia. *NEO* **2018**, *113*, 366–378. [[CrossRef](#)]
15. Finkel, T. Signal Transduction by Reactive Oxygen Species. *J. Cell Biol.* **2011**, *194*, 7–15. [[CrossRef](#)]
16. Marklund, S.L. Human Copper-Containing Superoxide Dismutase of High Molecular Weight. *Proc. Natl. Acad. Sci. USA* **1982**, *79*, 7634–7638. [[CrossRef](#)]
17. Oury, T.D.; Day, B.J.; Crapo, J.D. Extracellular Superoxide Dismutase in Vessels and Airways of Humans and Baboons. *Free Radic. Biol. Med.* **1996**, *20*, 957–965. [[CrossRef](#)]
18. Woo, H.A.; Yim, S.H.; Shin, D.H.; Kang, D.; Yu, D.-Y.; Rhee, S.G. Inactivation of Peroxiredoxin I by Phosphorylation Allows Localized H₂O₂ Accumulation for Cell Signaling. *Cell* **2010**, *140*, 517–528. [[CrossRef](#)]
19. Delaney, C.; Wright, R.H.; Tang, J.-R.; Woods, C.; Villegas, L.; Sherlock, L.; Savani, R.C.; Abman, S.H.; Nozik-Grayck, E. Lack of EC-SOD Worsens Alveolar and Vascular Development in a Neonatal Mouse Model of Bleomycin-Induced Bronchopulmonary Dysplasia and Pulmonary Hypertension. *Pediatr. Res.* **2015**, *78*, 634–640. [[CrossRef](#)]
20. Carlsson, L.M.; Jonsson, J.; Edlund, T.; Marklund, S.L. Mice Lacking Extracellular Superoxide Dismutase Are More Sensitive to Hyperoxia. *Proc. Natl. Acad. Sci. USA* **1995**, *92*, 6264–6268. [[CrossRef](#)] [[PubMed](#)]
21. Xu, D.; Guo, H.; Xu, X.; Lu, Z.; Fassett, J.; Hu, X.; Xu, Y.; Tang, Q.; Hu, D.; Somani, A.; et al. Exacerbated Pulmonary Arterial Hypertension and Right Ventricular Hypertrophy in Animals with Loss of Function of Extracellular Superoxide Dismutase. *Hypertension* **2011**, *58*, 303–309. [[CrossRef](#)]
22. Folz, R.J.; Abushama, A.M.; Suliman, H.B. Extracellular Superoxide Dismutase in the Airways of Transgenic Mice Reduces Inflammation and Attenuates Lung Toxicity Following Hyperoxia. *J. Clin. Investig.* **1999**, *103*, 1055–1066. [[CrossRef](#)]
23. Ahmed, M.N.; Suliman, H.B.; Folz, R.J.; Nozik-Grayck, E.; Golson, M.L.; Mason, S.N.; Auten, R.L. Extracellular Superoxide Dismutase Protects Lung Development in Hyperoxia-Exposed Newborn Mice. *Am. J. Respir. Crit. Care Med.* **2003**, *167*, 400–405. [[CrossRef](#)]
24. Perveen, S.; Patel, H.; Arif, A.; Younis, S.; Codipilly, C.N.; Ahmed, M. Role of EC-SOD Overexpression in Preserving Pulmonary Angiogenesis Inhibited by Oxidative Stress. *PLoS ONE* **2012**, *7*, e51945. [[CrossRef](#)]
25. Oury, T.D.; Day, B.J.; Crapo, J.D. Extracellular Superoxide Dismutase: A Regulator of Nitric Oxide Bioavailability. *Lab. Invest.* **1996**, *75*, 617–636.
26. Brady, T.C.; Chang, L.Y.; Day, B.J.; Crapo, J.D. Extracellular Superoxide Dismutase Is Upregulated with Inducible Nitric Oxide Synthase after NF-Kappa B Activation. *Am. J. Physiol.* **1997**, *273*, L1002–L1006. [[CrossRef](#)]
27. Friebe, A.; Schultz, G.; Koesling, D. Stimulation of Soluble Guanylate Cyclase by Superoxide Dismutase Is Mediated by NO. *Biochem. J.* **1998**, *335 Pt 3*, 527–531. [[CrossRef](#)]
28. Farrow, K.N.; Lakshminrusimha, S.; Reda, W.J.; Wedgwood, S.; Czech, L.; Gugino, S.F.; Davis, J.M.; Russell, J.A.; Steinhorn, R.H. Superoxide Dismutase Restores ENOS Expression and Function in Resistance Pulmonary Arteries from Neonatal Lambs with Persistent Pulmonary Hypertension. *Am. J. Physiol. Lung Cell. Mol. Physiol.* **2008**, *295*, L979–L987. [[CrossRef](#)]
29. Young, S.L.; Evans, K.; Eu, J.P. Nitric Oxide Modulates Branching Morphogenesis in Fetal Rat Lung Explants. *Am. J. Physiol. Lung Cell. Mol. Physiol.* **2002**, *282*, L379–L385. [[CrossRef](#)]
30. Han, R.N.N.; Stewart, D.J. Defective Lung Vascular Development in Endothelial Nitric Oxide Synthase-Deficient Mice. *Trends Cardiovasc. Med.* **2006**, *16*, 29–34. [[CrossRef](#)]
31. Bachiller, P.R.; Cornog, K.H.; Kato, R.; Buys, E.S.; Roberts, J.D. Soluble Guanylate Cyclase Modulates Alveolarization in the Newborn Lung. *Am. J. Physiol. Lung Cell Mol. Physiol.* **2013**, *305*, L569–L581. [[CrossRef](#)]

32. Parton, R.G.; del Pozo, M.A. Caveolae as Plasma Membrane Sensors, Protectors and Organizers. *Nat. Rev. Mol. Cell Biol.* **2013**, *14*, 98–112. [[CrossRef](#)]
33. Ahmed, M.N.; Codipilly, C.; Hogg, N.; Auten, R.L. The Protective Effect of Overexpression of Extracellular Superoxide Dismutase on Nitric Oxide Bioavailability in the Lung after Exposure to Hyperoxia Stress. *Exp. Lung Res.* **2011**, *37*, 10–17. [[CrossRef](#)] [[PubMed](#)]
34. Oshikawa, J.; Urao, N.; Kim, H.W.; Kaplan, N.; Razvi, M.; McKinney, R.; Poole, L.B.; Fukai, T.; Ushio-Fukai, M. Extracellular SOD-Derived H₂O₂ Promotes VEGF Signaling in Caveolae/Lipid Rafts and Post-Ischemic Angiogenesis in Mice. *PLoS ONE* **2010**, *5*, e10189. [[CrossRef](#)]
35. Shen, B.-Q.; Lee, D.Y.; Zioncheck, T.F. Vascular Endothelial Growth Factor Governs Endothelial Nitric-Oxide Synthase Expression via a KDR/Flk-1 Receptor and a Protein Kinase C Signaling Pathway*. *J. Biol. Chem.* **1999**, *274*, 33057–33063. [[CrossRef](#)]
36. Simons, M.; Gordon, E.; Claesson-Welsh, L. Mechanisms and Regulation of Endothelial VEGF Receptor Signalling. *Nat. Rev. Mol. Cell Biol.* **2016**, *17*, 611–625. [[CrossRef](#)]
37. Archer, S.L.; Johnson, G.J.; Gebhard, R.L.; Castleman, W.L.; Levine, A.S.; Westcott, J.Y.; Voelkel, N.F.; Nelson, D.P.; Weir, E.K. Effect of Dietary Fish Oil on Lung Lipid Profile and Hypoxic Pulmonary Hypertension. *J. Appl. Physiol.* **1989**, *66*, 1662–1673. [[CrossRef](#)]
38. Perez, M.; Lee, K.J.; Cardona, H.J.; Taylor, J.M.; Robbins, M.E.; Waypa, G.B.; Berkelhamer, S.K.; Farrow, K.N. Aberrant CGMP Signaling Persists during Recovery in Mice with Oxygen-Induced Pulmonary Hypertension. *PLoS ONE* **2017**, *12*, e0180957. [[CrossRef](#)]
39. Bradford, M.M. A Rapid and Sensitive Method for the Quantitation of Microgram Quantities of Protein Utilizing the Principle of Protein-Dye Binding. *Anal. Biochem.* **1976**, *72*, 248–254. [[CrossRef](#)]
40. Gupta, A.; Perez, M.; Lee, K.J.; Taylor, J.M.; Farrow, K.N. SOD2 Activity Is Not Impacted by Hyperoxia in Murine Neonatal Pulmonary Artery Smooth Muscle Cells and Mice. *Int. J. Mol. Sci.* **2015**, *16*, 6373–6390. [[CrossRef](#)]
41. Datta, A.; Kim, G.A.; Taylor, J.M.; Gugino, S.F.; Farrow, K.N.; Schumacker, P.T.; Berkelhamer, S.K. Mouse Lung Development and NOX1 Induction during Hyperoxia Are Developmentally Regulated and Mitochondrial ROS Dependent. *Am. J. Physiol. Lung Cell Mol. Physiol.* **2015**, *309*, L369–L377. [[CrossRef](#)] [[PubMed](#)]
42. Sherlock, L.G.; Trumpie, A.; Hernandez-Lagunas, L.; McKenna, S.; Fisher, S.; Bowler, R.; Wright, C.J.; Delaney, C.; Nozik-Grayck, E. Redistribution of Extracellular Superoxide Dismutase Causes Neonatal Pulmonary Vascular Remodeling and PH but Protects Against Experimental Bronchopulmonary Dysplasia. *Antioxidants* **2018**, *7*, 42. [[CrossRef](#)]
43. Yamakura, F.; Kawasaki, H. Post-Translational Modifications of Superoxide Dismutase. *Biochim. Biophys. Acta (BBA)–Proteins Proteom.* **2010**, *1804*, 318–325. [[CrossRef](#)] [[PubMed](#)]
44. Ma, Q. Role of Nrf2 in Oxidative Stress and Toxicity. *Annu. Rev. Pharmacol. Toxicol.* **2013**, *53*, 401–426. [[CrossRef](#)]
45. Ma, D.; Gao, W.; Liu, J.; Kong, D.; Zhang, Y.; Qian, M. Mechanism of Oxidative Stress and Keap-1/Nrf2 Signaling Pathway in Bronchopulmonary Dysplasia. *Medicine (Baltimore)* **2020**, *99*. [[CrossRef](#)]
46. Gerber, H.-P.; McMurtrey, A.; Kowalski, J.; Yan, M.; Keyt, B.A.; Dixit, V.; Ferrara, N. Vascular Endothelial Growth Factor Regulates Endothelial Cell Survival through the Phosphatidylinositol 3'-Kinase/Akt Signal Transduction Pathway: REQUIREMENT FOR Flk-1/KDR ACTIVATION*. *J. Biol. Chem.* **1998**, *273*, 30336–30343. [[CrossRef](#)]
47. Brown, K.R.S.; England, K.M.; Goss, K.L.; Snyder, J.M.; Acarregui, M.J. VEGF Induces Airway Epithelial Cell Proliferation in Human Fetal Lung in Vitro. *Am. J. Physiol. Lung Cell. Mol. Physiol.* **2001**, *281*, L1001–L1010. [[CrossRef](#)]
48. Hong, Y.A.; Lim, J.H.; Kim, M.Y.; Kim, Y.; Park, H.S.; Kim, H.W.; Choi, B.S.; Chang, Y.S.; Kim, H.W.; Kim, T.-Y.; et al. Extracellular Superoxide Dismutase Attenuates Renal Oxidative Stress Through the Activation of Adenosine Monophosphate-Activated Protein Kinase in Diabetic Nephropathy. *Antioxid. Redox Signal.* **2017**, *28*, 1543–1561. [[CrossRef](#)]
49. Wert, K.J.; Velez, G.; Cross, M.R.; Wagner, B.A.; Teoh-Fitzgerald, M.L.; Buettner, G.R.; McAnany, J.J.; Olivier, A.; Tsang, S.H.; Harper, M.M.; et al. Extracellular Superoxide Dismutase (SOD3) Regulates Oxidative Stress at the Vitreoretinal Interface. *Free Radic Biol. Med.* **2018**, *124*, 408–419. [[CrossRef](#)]
50. Kim, H.W.; Lin, A.; Guldberg, R.E.; Ushio-Fukai, M.; Fukai, T. Essential Role of Extracellular SOD in Reparative Neovascularization Induced by Hindlimb Ischemia. *Circ. Res.* **2007**, *101*, 409–419. [[CrossRef](#)]
51. Förstermann, U.; Sessa, W.C. Nitric Oxide Synthases: Regulation and Function. *Eur Heart J.* **2012**, *33*, 829–837. [[CrossRef](#)]